Model Predictive Control for Vehicle Stabilization at the Limits of Handling

Craig Earl Beal and J. Christian Gerdes

***Abstract*— Recent developments in vehicle steering systems offer new opportunities to measure the steering torque and reliably estimate the vehicle sideslip and the tire–road friction coefficient. This paper presents an approach to vehicle stabilization that leverages these estimates to define state boundaries that exclude unstable vehicle dynamics and utilizes a model predictive envelope controller to bound the vehicle motion within this stable region of the state space. This approach provides a large operating region accessible by the driver and smooth interventions at the stability boundaries. Experimental results obtained with a steer-by-wire vehicle and a proof of envelope invariance demonstrate the efficacy of the envelope controller in controlling the vehicle at the limits of handling.**

***Index Terms*— Driver assistance, envelope control, model predictive control (MPC), vehicle dynamics, vehicle safety.**

I. Introduction

EVERY year, thousands of lives are lost in vehicle crashes due to loss of control by the driver. In some of these loss-of-control incidents, timely and accurate application of control inputs would stabilize the vehicle and provide sufficient assistance to the driver to completely avoid a crash. Current state-of-the-art electronic stability control (ESC) systems are designed to accomplish this task. Results of studies on these stability control systems demonstrate that they are highly effective in preventing many of these loss-of-control incidents, leading to an estimated 30% reduction in fatal accidents in vehicles equipped with ESC [1].

Fundamentally, the role of a stability control system is to prevent the vehicle from deviating significantly from the behavior intended by the driver. However, this task is challenging because the true intent of the driver may be infeasible given the handling limits of the vehicle, which in any case cannot be measured. Therefore, the control system cannot simply track the driver's intent and the problem must be phrased in an alternate manner. For production stability control systems, driver intent is addressed by inferring the desired vehicle behavior from a linear model and a limited set of sensor measurements [2]. These measurements are combined with estimates of the states and tire–road friction coefficient and are compared with the linear model. Control action is taken if there is significant deviation. This control scheme is highly effective, as seen from National Highway Traffic Safety Administration analysis, and is robust despite the limited sensor suite it utilizes. However, the reliance on deviation from a linear model has two drawbacks. The first is that the stability control system allows only dynamics that are close to the linear model, while skilled drivers may be able to access other handling regimes. The second is that, in order to avoid unnecessary interventions, the system must not take action until the vehicle behavior is measurably outside of the stable regime.

While these types of tradeoffs are required in a system for which it is feasible to install on production vehicles, a number of technologies that have the capability of providing additional information and actuation to stability control systems are appearing on the market. Among these enabling technologies are electric power steering and steer-by-wire systems. With these actuators comes the ability to measure steering torque and, with it, the ability to accurately estimate both the tire–road friction coefficient and the vehicle sideslip angle [3].

With estimates of the states and friction characteristics available, it is possible to take a different approach to vehicle stabilization. Most drivers are aware that there exist inherent limitations in tire grip and therefore in the vehicle handling capabilities. Very highly skilled drivers can operate the vehicle at these limits without allowing the vehicle to become unstable. However, less skilled drivers may exceed these handling limits without realizing it, perhaps due to aggressive driving or emergency maneuvering. With full-state feedback available, the stability control system can accurately estimate these limitations and assist the driver in maintaining the vehicle inside the bounds of the vehicle capabilities. Thus, the system may be referred to as an "envelope control" system, similar to the envelope protection systems used in modern commercial aircraft [4]. Hsu and Gerdes demonstrated one such system that used a front steer-by-wire technique for actuation and prevented the vehicle from exceeding front and rear axle slip angle thresholds [5].

Phrased in this envelope control formulation, the control task is well-matched to the structure of model predictive control (MPC), where at each time step the controller action is the solution to an optimization problem. Thus, model predictive control offers a method for incorporating both an objective as well as constraints. Taken in the context of the stabilization problem, the objective can be leveraged to express the driver's intended vehicle behavior while the constraints represent the physical limitations of the vehicle. Therefore, the

Manuscript received March 26, 2011; revised November 24, 2011; accepted April 10, 2012. Manuscript received in final form May 15, 2012. Date of publication July 6, 2012; date of current version June 14, 2013. Recommended by Associate Editor M. Mattei. This work was supported in part by Nissan Motor Company, Ltd., Kanagawa, Japan.

C. E. Beal was with the Department of Mechanical Engineering, Stanford University, Stanford, CA 94305 USA. He is now with Bucknell University, Lewisburg, PA 17837 USA (e-mail: cbeal@bucknell.edu).

J. C. Gerdes is with the Department of Mechanical Engineering, Stanford University, Stanford, CA 94305 USA (e-mail: gerdes@stanford.edu).

Color versions of one or more of the figures in this paper are available online at http://ieeexplore.ieee.org.

Digital Object Identifier 10.1109/TCST.2012.2200826

controller responds as desired, allowing the driver full freedom to control the vehicle away from the boundaries but providing the necessary assistance to prevent the vehicle from exiting the safe handling envelope. In this paper, the envelope controller utilizes a handling envelope derived from experimentation and phase-plane analysis to provide the yaw rate and rear slip angle boundaries appropriate to the vehicle dynamics at the limits of handling. Using these boundaries, the MPC scheme provides refined control action at the boundaries of the envelope.

Several authors have suggested model predictive techniques to control vehicle behavior in earlier work. Falcone *et al*. presented investigations on the use of MPC for autonomous driving when the desired vehicle path is known *a priori* [6], [7]. Palmieri *et al*. developed a model predictive regulator to decrease excessive yaw rate or sideslip angle beyond a pair of thresholds [8], and Bernardini *et al*. presented a reference tracking controller with tire slip limits [9]. While these authors focused on autonomous operation and reference tracking, the approach taken here uses MPC to define and enforce a safe handling envelope in which the driver can maneuver.

Common to all of these schemes is the issue of modeling the nonlinear vehicle behavior for control. Since critical driver assistance situations typically occur at the limits of handling, a linear model of the tire behavior results in significant modeling error and poor controller performance. Models that represent the full nonlinear dynamics, however, present problems in terms of practical constraints such as computational time and parameter uncertainty in addition to the possibility of producing emergent behaviors. As a result, Falcone |itet al. used a full nonlinear tire model in simulation but approximated this model with linearizations for real-time operation [6]. Palmieri *et al*. linearized the equations of motion for the combined system of the vehicle and the tires [8], and Bernardini *et al*. used a piecewise linear representation of the tire forces [9]. In this paper, the input is formulated as the front lateral force, rather than the steering angle. As a result, the input nonlinearity is extracted rather than linearized and the control action is more precise, leading to close adherence to the envelope boundaries in operation.

This paper outlines the development of a safe handling envelope and the formulation of an MPC strategy. This envelope control scheme utilizes real-time state measurements for feedback and front steering as actuation to modify the vehicle behavior. Experiments with a steer-by-wire test vehicle on a low-friction surface demonstrate the ability of the controller to provide smooth interventions to keep the vehicle inside the envelope and preserve stability. A selection of these results is presented in this paper, along with discussion of the controller behavior and a proof of the invariance of the envelope under the model predictive controller.

II. Vehicle Models

Two models of the vehicle were used in the development of the model predictive envelope controller: the linear bicycle model, and the affine force-input (AFI) model. In this paper, the linear bicycle model is used to develop a reference trajectory of the vehicle behavior, while the AFI model is used to formulate the model predictive controller.

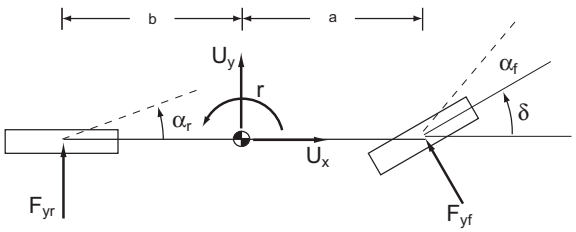

Fig. 1. Bicycle model.

A. Linear Bicycle Model

The bicycle model considered in this paper is a simplified two-state model of the vehicle dynamics which yields a pair of linear equations that describe the rotational and lateral velocities of the vehicle. The model, which is illustrated in Fig. 1, utilizes small angle assumptions and the approximation that the tires on each axle can be lumped together. A constant vehicle longitudinal velocity U_x is also assumed. The equations of motion for this model can be written as

$$\dot{\beta} = \frac{F_{yf} + F_{yr}}{mU_x} - r, \qquad \dot{r} = \frac{aF_{yf} - bF_{yr}}{I_{zz}} \tag{1}$$

where β is the ratio of the lateral to the longitudinal velocity, and the parameters m and I_{zz} are the vehicle mass and yaw moment of inertia, respectively. For the linear bicycle model, a linear tire model is also assumed, yielding the following expressions for the front and rear tire forces:

$$F_{yf} = -C_{\alpha f}\alpha_f, \qquad F_{yr} = -C_{\alpha_r}\alpha_r \tag{2}$$

where α_f and α_r are described in terms of the vehicle states and the steering angle input from the driver is

$$\alpha_f = \beta + \frac{ar}{U_x} - \delta, \qquad \alpha_r = \beta - \frac{br}{U_x}. \tag{3}$$

Substituting (3) into (2) and then into (1) yields a description of the system that specifies the behavior of the states if the driver input is known. This system can be written in state-space form as $\dot{x} = Ax + B\delta$ with $x = [\beta\ r]^T$ and

$$A = \begin{bmatrix} \frac{-(C_{af}+C_{ar})}{mU_x} & \frac{-(aC_{af}-bC_{ar})}{mU_x^2} - 1 \\ \frac{-(aC_{af}-bC_{ar})}{I_{zz}} & \frac{-(a^2C_{af}+b^2C_{ar})}{I_{zz}U_x} \end{bmatrix}$$
$$B = \begin{bmatrix} \frac{C_{af}}{mU_x} \\ \frac{aC_{af}}{I_{zz}} \end{bmatrix}. \tag{4}$$

B. AFI Model

The AFI model describes the same states as the bicycle model from the previous section and is based on the same small angle and lumped-axle assumptions as the bicycle model shown in Fig. 1. Again, the model is derived from the equations of motion given by (1). In contrast to the bicycle model, F_{yf} is chosen rather than δ as the input. For the rear axle, the lateral force F_{yr} is linearized about the slip angle operating point. This linearization is found by taking the zeroth- and first-order terms of the Taylor expansion of any smooth tire model, from which the tire force $\overline{F}_{yr}$ and the

local cornering stiffness $\widetilde{C}_{\alpha_r}$ can be found at the operating point $\overline{\alpha}_r$

$$F_{yr} = \overline{F}_{yr} - \widetilde{C}_{\alpha_r}(\alpha_r - \overline{\alpha}_r). \tag{5}$$

This rear tire force equation is affine in the rear slip angle α_r, which preserves the convexity of the model and also gives a representation of the nonlinear tire force behavior. For use in the model predictive controller, this linearization is assumed to provide a reasonable approximation of the rear tire behavior over a short prediction horizon. Substituting (5) into (1) yields

$$\begin{aligned}\dot{\beta} &= \frac{F_{yf} + \overline{F}_{yr} - \widetilde{C}_{\alpha_r}(\alpha_r - \overline{\alpha}_r)}{mU_x} - r \\ \dot{r} &= \frac{aF_{yf} - b\left[\overline{F}_{yr} - \widetilde{C}_{\alpha_r}(\alpha_r - \overline{\alpha}_r)\right]}{I_{zz}}.\end{aligned} \tag{6}$$

Like the bicycle model, $\alpha_r = \beta - (b/U_x)r$, which yields

$$\begin{aligned}\dot{\beta} &= \frac{F_{yf} + \overline{F}_{yr} - \widetilde{C}_{\alpha_r}\left(\beta - \frac{b}{U_x}r - \overline{\alpha}_r\right)}{mU_x} - r \\ \dot{r} &= \frac{aF_{yf} - b\left[\overline{F}_{yr} - \widetilde{C}_{\alpha_r}\left(\beta - \frac{b}{U_x}r - \overline{\alpha}_r\right)\right]}{I_{zz}}.\end{aligned} \tag{7}$$

A state-space description of the system needed for use in the MPC problem can be defined as $\dot{x} = A(t)x + BF_{yf} + d(t)$, where, again, $x = [\beta\ r]^T$ with

$$\begin{aligned}A(t) &= \begin{bmatrix} -\frac{\widetilde{C}_{\alpha_r}}{mU_x} & \frac{b\widetilde{C}_{\alpha_r}}{mU_x^2} - 1 \\ \frac{b\widetilde{C}_{\alpha_r}}{I_{zz}} & -\frac{b^2\widetilde{C}_{\alpha_r}}{U_x I_{zz}} \end{bmatrix} \\ B &= \begin{bmatrix} \frac{1}{mU_x} \\ \frac{a}{I_{zz}} \end{bmatrix} \\ d(t) &= \begin{bmatrix} \frac{(\overline{F}_{yr} + \widetilde{C}_{\alpha_r}\overline{\alpha}_r)}{mU_x} \\ \frac{-b(\overline{F}_{yr} + \widetilde{C}_{\alpha_r}\overline{\alpha}_r)}{I_{zz}} \end{bmatrix}.\end{aligned} \tag{8}$$

C. Lateral Fiala Tire Model

Examining the equations of motion for the AFI model, it is clear that, even if the driver input is given, the state trajectories cannot be calculated solely from the equations given. The AFI model relies on an external tire model to provide estimates of lateral tire force $\left(\overline{F}_{yr}\right)$ and local cornering stiffness $\left(\widetilde{C}_{\alpha_r}\right)$ given the slip angle $(\overline{\alpha}_r)$ for the rear tire at each time step.

A brush tire model, for which the response is illustrated in Fig. 2, provides this force information. The model uses a parabolic pressure distribution such as the one by Fiala [10] and others, but incorporates separate peak and sliding friction coefficients. The model is parameterized by the linear cornering stiffness (C_α), the peak force (μF_z), and the ratio of the sliding friction coefficient to the peak coefficient (R_μ).

The relationship between the slip angle and the tire force is given by the following expression if the tire is operating at a slip angle equal to or less than the angle of full sliding:

$$\begin{aligned}F_y = {} & C_\alpha \tan\alpha - \frac{C_\alpha^2}{3\mu F_z}(2 - R_\mu)\tan\alpha\,|\tan\alpha| \\ & + \frac{C_\alpha^3}{9(\mu F_z)^2}\left(1 - \frac{2}{3}R_\mu\right)\tan^3\alpha.\end{aligned} \tag{9}$$

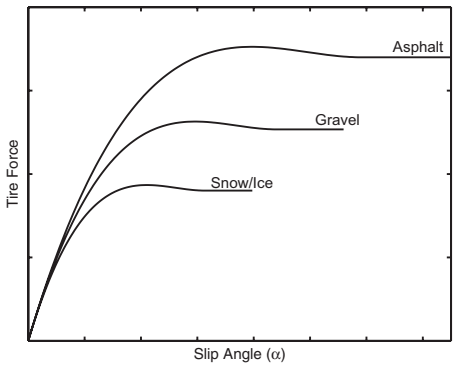

Fig. 2. Tire curve: two-coefficient Brush model.

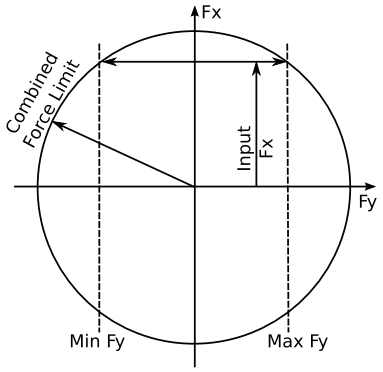

Fig. 3. Combined tire force limits.

Since this equation is a cubic polynomial, it is possible to calculate slip angle from lateral force, but an additional assumption that the tire is operating at an angle equal to or below the slip angle corresponding to the peak force is necessary to obtain a single solution. This assumption is justified by the later use of this equation where the front axle operating point is chosen to be between the positive and negative peak slip angles. A relationship for the local cornering stiffness may be derived from the force model by direct differentiation.

Several explicit relationships also may be derived for a tire at the angle of peak force generation. The resulting equations (used in developing the control strategy in the following sections) are

$$q = \left(1 - \frac{2}{3}R_\mu\right)^{-1} \tag{10}$$

$$F_{y_{\max}} = \mu F_z\left(-q + \frac{2 - R_\mu}{3}q^2 - \frac{1 - \frac{2}{3}R_\mu}{9}q^3\right) \tag{11}$$

$$\alpha_{\max} = \arctan\left(\frac{q\mu F_z}{C_\alpha}\right). \tag{12}$$

This tire model also provides a mechanism for including the effects of lateral–longitudinal force coupling. In general, the force demand on a tire is a vector sum of the lateral and longitudinal components and must be less than the total available force

$$F_{\text{tot}} = \sqrt{F_x^2 + F_y^2} \le \mu F_z. \tag{13}$$

Therefore, it is possible to view the F_x demand as an input that dictates the maximum available F_y force, as illustrated in Fig. 3. This "derating" approach can be expressed as

$$\mu F_z = \sqrt{(\mu F_z)_{\text{nom}}^2 - F_x^2} \tag{14}$$

and the adjusted value of μF_z can be used as a parameter for the brush tire model to yield an approximation of the coupled tire force. For longitudinal forces significantly smaller than $(\mu F_z)_{\text{nom}}$, this is a relatively good model, but the lack of longitudinal slip information makes the relationship incomplete. For practical purposes, μF_z is bounded away from zero to improve the model performance.

III. Control Strategy

The envelope controller presented in this paper is designed to achieve two primary objectives. The first is that the controller must keep the vehicle inside the handling envelope and respond appropriately in the event that a disturbance causes the vehicle to leave the envelope. The second objective is for the controller to track the driver's intended vehicle behavior inside the envelope and behave in a predictable manner when at or beyond the envelope boundaries.

Since a model predictive controller operates by solving an optimization problem to determine a set of inputs that satisfies an objective and any constraints over a specified control time horizon at each control time step, MPC provides a straightforward method of implementing an envelope control strategy. In the MPC framework, tracking the driver's desired trajectory becomes the objective, while the envelope boundaries and actuator limits are the constraints. Furthermore, after finding the optimal input sequence, the first input in the sequence is applied to the system and the process is started again. In this manner, the optimization routine needs only to find an open-loop optimal set of inputs, but the resampling and recomputation at each time step provide a feedback loop to take into account deviations from the optimal trajectory from disturbances or model error, for example. The following subsections describe how an envelope control scheme can be implemented in an MPC formulation.

A. MPC With the AFI Model

The rationale for using the AFI model to implement the model predictive controller can be explained by examining the equations of motion for the single-track model, given here again as (15). It is obvious by inspection that the equations are linear in the front and rear lateral forces

$$\dot{\beta} = \frac{\boldsymbol{F_{yf}} + \boldsymbol{F_{yr}}}{mU_x} - r, \qquad \dot{r} = \frac{a\boldsymbol{F_{yf}} - b\boldsymbol{F_{yr}}}{I_{zz}}. \tag{15}$$

The controller design presented in this paper assumes a vehicle with rear wheel drive and front steering, where the controller has the authority to augment the driver's steering command up to the limits of the actuators. In this configuration, the drive torques and steering are on separate axles and so the tires on the front axle generate only lateral forces. Therefore, a manipulation of the steering can be seen simply as a state-dependent front lateral force command. Taking this abstraction a bit further, the front lateral force can be viewed by the optimization solver as the input to the system rather than the front steering angle. Thus, by changing variables, the nonconvex relationship between front lateral force and steering angle is extracted outside the optimization solver as seen in Fig. 4, maintaining the ability to rapidly solve the problem while preserving the characteristics of the desired tire model.

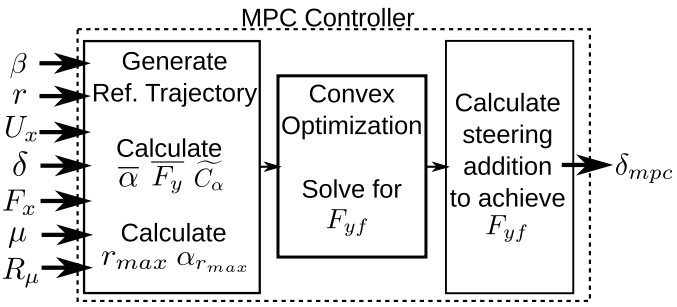

Fig. 4. MPC block diagram.

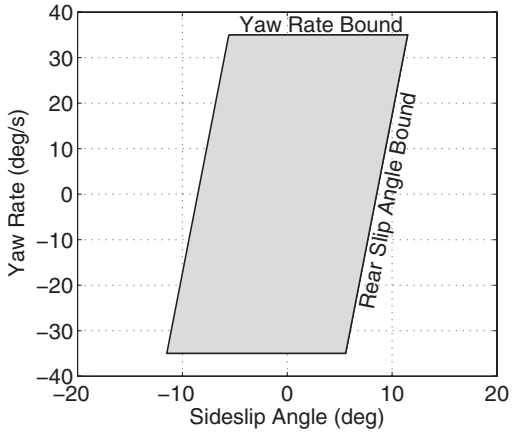

Fig. 5. MPC envelope controller boundaries.

Unfortunately, this technique does not work on the rear axle of the vehicle because of the lack of actuation. The rear lateral tire force is a function of the vehicle states and the longitudinal slip. Worse, this function is nonconvex and is needed to accurately calculate the predicted model states in the optimization routine. As a result, the rear tire linearization in (5) is used. With the pre-solve and post-solve steps illustrated in Fig. 4, the resulting optimization problem is convex and thus can be solved robustly and rapidly through the use of well-known convex optimization techniques [11].

B. Envelope Boundaries

The envelope for this controller is a parallelogram in state space, as seen in Fig. 5. The envelope boundaries are computed using an approximation of the tire–road friction coefficient, which is assumed to be estimated in real time. It is not expected that an exact value of the friction coefficient will be known, particularly since it is likely to be varying frequently with the changing road surface as in the experimental results. The first envelope constraint is computed from the steady-state yaw rate associated with the estimated maximum tire forces. From (1) at steady state, the tire forces in equilibrium satisfy

$aF_{yf_{\text{eq}}} = bF_{yr_{\text{eq}}}$ and the equilibrium yaw rate can be expressed in terms of the front or rear equilibrium tire force as

$$r_{\text{eq}} = \frac{F_{yr_{\text{eq}}}(1 + b/a)}{mU_x} = \frac{F_{yf_{\text{eq}}}(1 + a/b)}{mU_x} \tag{16}$$

where the equilibrium force can be determined by comparing the magnitude of the moments produced by the maximum tire forces on each axle of the vehicle. This yields the following set of yaw rate limits:

$$r_{\max} = \begin{cases} \frac{F_{yr\max}(1+b/a)}{mU_x} & F_{yf_{\max}} \geq \frac{b}{a}F_{yr_{\max}} \\ \frac{F_{yf\max}(1+a/b)}{mU_x} & F_{yf_{\max}} < \frac{b}{a}F_{yr_{\max}}. \end{cases} \tag{17}$$

To close the envelope in the state plane, a second set of constraints that limit the sideslip angle are needed. However, a simple limit on the sideslip angle has significant drawbacks when considering the sideslip angle dependence on speed and vehicle parameterization. However, the slip angle of the rear tire scales naturally with speed and also includes the effect of yaw rate, limiting the sideslip angle at high yaw rates. Given estimates of the vehicle cornering stiffness and the tire–road friction coefficients, (12) specifies the angle associated with the maximum tire force generation. Using this angle to set the maximum rear slip angle yields a conservative envelope in which the vehicle maintains rear tire grip. However, highly skilled drivers can maintain vehicle stability while the rear tires attain large slip angles. The same is true of the envelope controller, and this performance can be achieved by choosing the rear slip angle boundary to be a few degrees past the peak. In practical testing, experienced drivers preferred the wider rear slip angle boundaries and enjoyed being able to stably slide the vehicle with the assistance of the controller.

C. Tracking Driver Intent

Stabilizing the vehicle is an important function of an envelope controller, but to assist the driver in guiding the vehicle along a safe trajectory the envelope controller also utilizes a tracking objective. There are a limited number of sensors available in production vehicles that yield information about the driver's intended vehicle behavior. Thus, the control design assumes that the driver's intended yaw rate and sideslip can be inferred by holding the steering angle and vehicle speed constant and propagating a linear bicycle model over a 150-ms control horizon to determine the target states to use for tracking. Away from the envelope boundaries, the linear model matches the vehicle behavior well. Since the vehicle is well away from the boundaries of the envelope and the tracking error is very small, the steering correction calculated by the model predictive controller will be very close to zero. Thus, the structure of the problem renders the controller silent away from the boundaries, providing an alternative to the use of logic to switch the controller on and off and allowing for progressive control action near the limits of handling.

D. Controller Implementation

When described as a control problem for MPC, the output of the controller at each time step is the solution to the optimization problem described here

$$\begin{aligned}
\text{minimize} \quad & \sum_{k=1}^{N} \left|\left| x_{\text{opt}}^k - x_{\text{des}}^k \right|\right|_{W_x}^2 + \ \ldots && \text{(18a)} \\
& \sum_{k=1}^{N-1} \ \left|\left| F_{yf}^k \right|\right|_{W_u}^2 + \eta \sum_{k=1}^{N} \left|\left| s_{\text{opt}}^k \right|\right|_1 \\
\text{s.t} \quad & x_{\text{opt}}^1 = A_d x_{\text{init}} + B_d F_{yf_{\text{init}}} && \text{(18b)} \\
& x_{\text{opt}}^{k+1} = A_d x_{\text{opt}}^k + B_d F_{yf}^k + d_d && \text{(18c)} \\
& k = 1, \ldots, N-1 \\
& F_{yf_{\min}} \leq F_{yr}^k \leq F_{yf_{\max}} \quad k = 1, \ldots, N-1 && \text{(18d)} \\
& \left| F_{yf}^k - F_{yf}^{k+1} \right| \leq F_{yf_{\text{slew}}} \quad k = 1, \ldots, N-2 && \text{(18e)} \\
& C_{\text{lim}} \left| x^k \right| \leq x_{\text{lim}} + s_{\text{opt}}^k \quad k = 1, \ldots, N && \text{(18f)} \\
& s_{\text{opt}}^k \geq 0, \quad k = 1, \ldots, N. && \text{(18g)}
\end{aligned}$$

Each term in this optimization statement has physical meaning in terms of the functionality of the envelope control system. The first term in the objective function (18a) represents the tracking objective. Thus, error between the solution trajectory and the desired linear behavior is penalized through a weighted norm. This ensures that the optimal control input tracks the driver's desired behavior. The second term in the input is a weighted norm on the inputs. For the controller described here, the only input to the system is F_{yf}, but, by defining the function as a weighted norm on the inputs, the problem may be extended to additional actuators. The final term in the objective function is a penalty on the slack variables that are added to the problem to ensure that the constraints do not cause the problem to become infeasible.

The dynamic constraints (18b)–(18c) describe the dynamics that the solution trajectory must obey. These dynamics are obtained by discretizing the continuous AFI system given in (8). A Tustin discretization method is used since it offers a closed-form solution that can easily be implemented in real time. The third constraint, i.e., (18d), restricts the MPC solver to a range of inputs that are achievable given the estimated friction coefficients and normal load on the front axle. Similarly, (18e) restricts the maximum change in the lateral force so that the actuator slew rate limits are respected. Finally, (18f) implements the constraints that define the boundaries of the envelope. Since yaw rate is one of the system states and rear slip angle is a linear combination of yaw rate and sideslip angle, the limit calculation matrix C_{lim} and the limit vector x_{lim} are

$$C_{\text{lim}} = \begin{bmatrix} 0 & 1 \\ 1 & -\frac{b}{Ux} \end{bmatrix}, \quad x_{\text{lim}} = \begin{bmatrix} r_{\text{lim}} \\ \alpha_{r_{\text{lim}}} \end{bmatrix}. \tag{19}$$

The optimization problem that results from the envelope controller is convex, as seen by inspection of the terms, and thus a specific set of embedded convex optimization tools can be brought to bear on the problem. Using a software such as described in [12] and [13], custom C-code is generated which can solve the model predictive envelope control problem with a 15-step horizon in under 2 ms on a single core of an Intel Core2 Duo processor. Despite fast solution techniques, this solve step requires nontrivial computation time, so delay

Fig. 6. P1 steer and drive-by-wire research testbed.

TABLE I
PARAMETERS FOR THE P1 TEST VEHICLE

Parameter	Symbol	Value	Units
Vehicle mass	m	1724	kg
Yaw moment of inertia	I_{zz}	1100	$\frac{\text{kg}}{\text{m}^2}$
Wheelbase	L	2.5	m
Front axle-CG distance	a	1.35	m
Rear axle-CG distance	b	1.15	m
Front cornering stiffness	$C_{\alpha f}$	90 000	$\frac{N}{\text{rad}}$
Rear cornering stiffness	$C_{\alpha r}$	138 000	$\frac{N}{\text{rad}}$

compensation is also added to the controller as described in [14]. This is expressed in the problem formulation by (18b), where the states after one time step are dictated solely by the initial conditions. By doing this, the MPC problem is solved not for the time step at initiation of the solver, but rather a solution is computed for the following time step when the inputs can be applied.

IV. EXPERIMENTAL APPARATUS

To examine the behavior of the controller described in the previous sections, experiments were performed with a fully drive-by-wire research testbed built by students at Stanford University. This vehicle, referred to as P1 and shown in Fig. 6, is a rear-wheel drive vehicle powered by independent left and right electric drive motors. P1 is also equipped with a pair of global positioning systems (GPSs) that provide velocity and attitude information that is fused with inertial measurements to achieve high-accuracy full-state feedback at a 500-Hz update rate, as described in [15]. The steering system includes independent left- and right-wheel actuation with high bandwidth response, as detailed in [16], and the handling properties of P1 are consistent with those of a sports sedan—with one important exception—and are detailed in Table I.

The exception to the normal vehicle handling properties for P1 is the yaw moment of inertia. Compared to the vehicle mass, wheelbase, and track width, the moment of inertia is unusually small. In addition, the drive system of P1 provides regenerative braking on the rear axle when the driver lifts off the accelerator pedal. The combination of these properties results in the vehicle being highly sensitive to accelerator inputs by the driver while cornering. In open-loop driving with the vehicle on a low-friction surface, drivers are often unable to stabilize the vehicle in oversteer events induced by the drive torque.

TABLE II
ENVELOPE CONTROLLER PARAMETERS

Parameter	Symbol	Value
MPC horizon	N	15
MPC time step	ΔT	0.01 s
Sideslip tracking weight	W_{x_β}	$5\frac{1}{\text{rad}}$
Yaw rate tracking weight	W_{x_r}	$50\frac{\text{s}}{\text{rad}}$
Input penalty weight	$W_{F_{yf}}$	$1 \times 10^{-5}\frac{1}{N}$
Slack variable penalty	η	5×10^4
Input limit	δ_{lim}	$\pm 22°$
Input slew rate limit	δ_{slew}	$\pm 140°/\text{s}$
Yaw rate limit	r_{lim}	††
Rear slip limit	$\alpha_{r_{\text{lim}}}$	††
Static friction coefficient	μ	0.6
Sliding friction coefficient	μ_s	0.55

†† Parameter is computed in real-time before optimization step.

For the experimental validation, tests were performed on surfaces comprised of mixed dirt, gravel, and asphalt. The friction characteristics of the surfaces were therefore highly variable. Some sections with very little loose dirt and gravel had normal adhesive friction characteristics of asphalt, while other sections with a lot of gravel would allow the tires to slide quite a bit. The variation in the distribution of loose particles on the surface was estimated to have a length scale on the order of tens of centimeters and at speed, an average friction coefficient of 0.6 was a suitable estimate. The friction information, as well as the sideslip and yaw rate states, could be estimated in real time using the technique described in [17], but a static *a priori* estimate of the friction properties and GPS-based state estimation were used to isolate the controller behavior from any undesired estimator-controller interactions.

V. RESULTS AND DISCUSSION

The first set of results with the model predictive envelope controller are shown in Fig. 7. This test was designed to excite the vehicle dynamics with steering input at roughly constant speed such that an uncontrolled vehicle would have left the envelope. To ensure consistent clean excitation of the vehicle steering, the sinusoidal driver steering input was generated using the vehicle computer. The envelope control parameters are shown in Table II, while the results are illustrated in Fig. 7(a)–(d), where Fig. 7(a) shows the vehicle states throughout the maneuver. The surface friction coefficient was estimated to be approximately 0.55–0.6, and so it is clear that the vehicle is very close to the maximum lateral acceleration on each phase of the sinusoidal maneuver.

Fig. 7(b) shows the limited quantities along with the dynamically calculated envelope boundaries. Because the boundaries are dependent upon vehicle speed, friction coefficients, and rear-wheel torque, all of which are held nearly constant, little variation in the limits occurs through the maneuver.

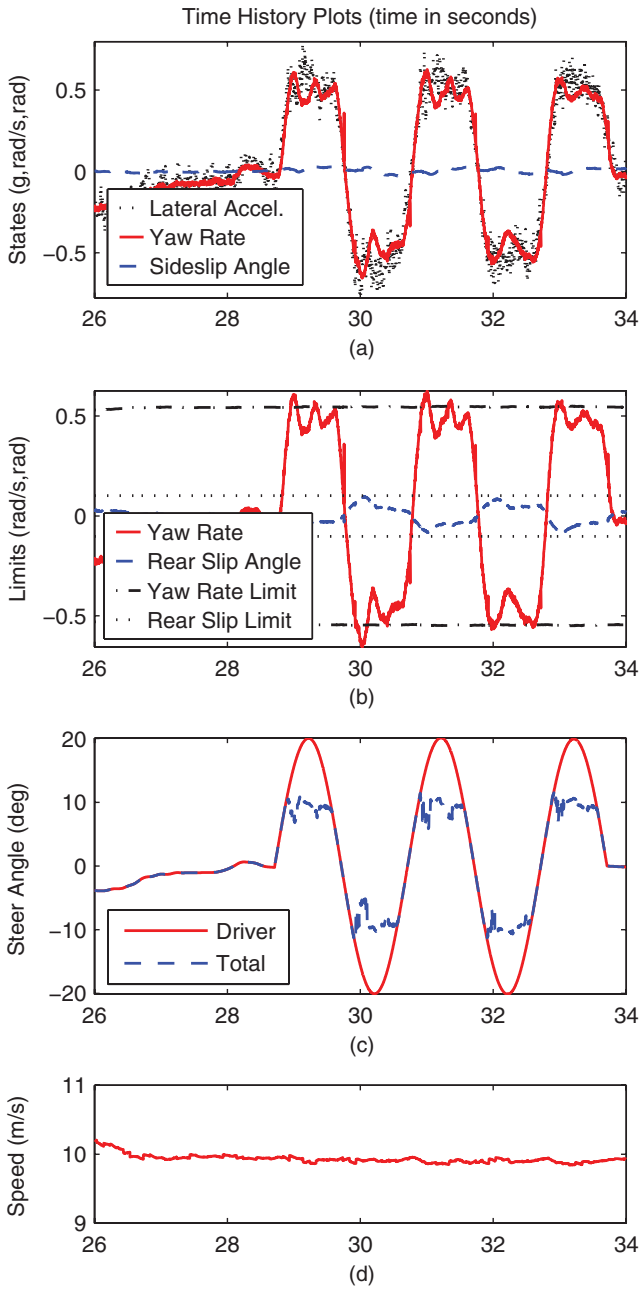

Fig. 7. Experimental slalom results. (a) Vehicle yaw rate, sideslip, and lateral acceleration. (b) Limited quantities and limits. (c) Driver and total steering angles. (d) Vehicle speed.

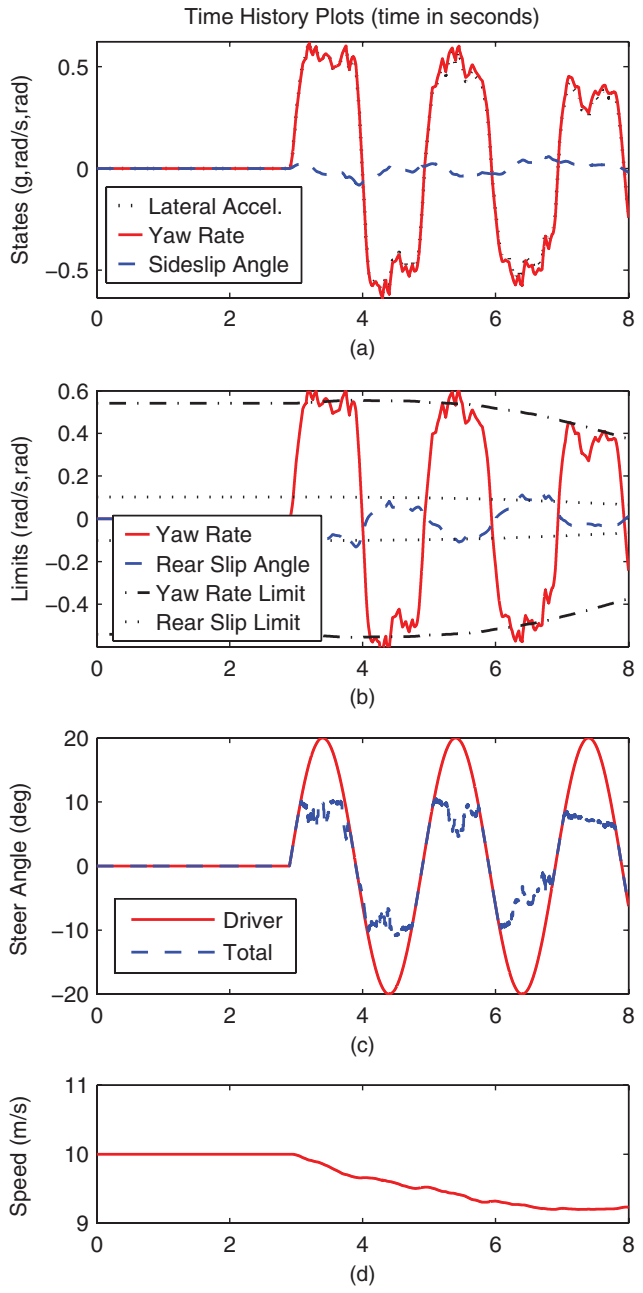

Fig. 8. Simulated slalom results. (a) Vehicle yaw rate, sideslip, and lateral acceleration. (b) Limited quantities and limits. (c) Driver and total steering angles. (d) Vehicle speed.

On examining the limited quantities, it is clear that, aside from a slight overshoot of the yaw rate, the controlled vehicle remains within the envelope boundaries. However, the advantage of the envelope controller goes beyond preventing major excursions of the vehicle states outside of the envelope. Using the AFI model to predict the vehicle behavior, the controller is capable of holding the vehicle very close to the boundaries. Assuming that the boundaries are set at the maximum capabilities of the vehicle, the controller is capable of assisting the driver in utilizing all of the vehicle's cornering capability while maintaining stability.

Fig. 7(c) shows the sinusoidal driver steering command as well as the total command that is applied to the front wheels after the controller steering addition. In this case, the driver command would cause the vehicle to exceed the boundaries of the envelope and so the controller countersteers to compensate. An important point here is that, because of the continuous nature of the controller, the system smoothly resumes the driver command once the driver steering angle results in states attainable inside the envelope. Therefore, there is no lag in the steering if the driver chooses to reverse the turning direction of the vehicle.

One other feature in the datasets seen particularly in the yaw rate and steering signals of Fig. 7 is an oscillation around the limit. Because the gravel is unevenly distributed on the test surface, this oscillation reflects the controller response to

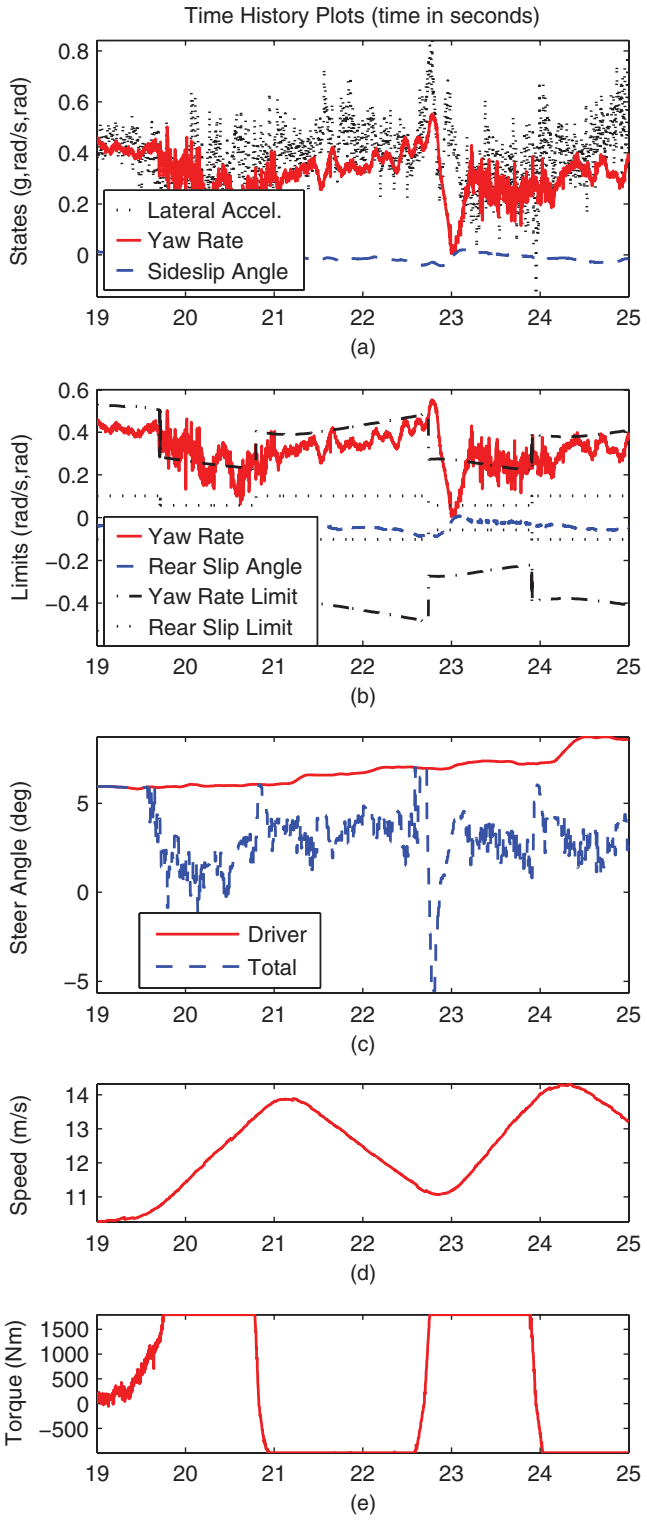

Fig. 9. Torque Input. (a) Vehicle yaw rate, sideslip, and lateral acceleration. (b) Limited quantities and limits. (c) Driver and total steering angles. (d) Vehicle speed. (e) Estimated rear-axle torque.

disturbances. This can be confirmed with a simulation run where the grip properties of each wheel are chosen from a random distribution.

The conditions for the simulation were set as closely as possible to match those of the experimental slalom shown in Fig. 7, including identical controller parameters. The friction coefficients were varied independently for each wheel every 0.04 s to represent the effect of unevenly distributed gravel. At the vehicle speed of 10 m/s, this equates to a 40-cm length scale for the friction variation. The distribution was assumed to be uniformly random, within the ranges $\mu = 0.6 \pm 0.4$ and $\mu_s = 0.55 \pm 0.4$. Since the friction coefficient μ always appears in the lateral tire force expression given in (9) as a product with normal force, this variation can also represent the changing normal load on a wheel.

TABLE III
ENVELOPE CONTROLLER PARAMETERS

Parameter	Symbol	Value
MPC horizon	N	15
MPC time step	ΔT	0.01 s
Sideslip tracking weight	W_{x_β}	$5\frac{1}{\text{rad}}$
Yaw rate tracking weight	W_{x_r}	$50\frac{\text{s}}{\text{rad}}$
Input penalty weight	W_δ	$1\frac{1}{\text{rad}}$
Slack variable penalty	η	5×10^4
Input limit	δ_{lim}	$\pm 22°$
Input slew rate limit	δ_{slew}	$\pm 140°/\text{s}$
Front slip limit	$\alpha_{f_{\text{lim}}}$	$\pm 8°$
Rear slip limit	$\alpha_{r_{\text{lim}}}$	$\pm 8°$

Once the random friction conditions were incorporated into the simulation framework, oscillations of approximately the same magnitude and frequency as in the experiments were observed. This is particularly apparent when looking at the first two cycles of slalom in Figs. 7(c) and 8(c), where the total steering command is plotted. Similar effects are also seen in Figs. 7(b) and 8(b), where the yaw rate and rear slip angles show this same oscillatory behavior.

The previous two sets of results demonstrate the vehicle behavior when primarily excited with steering input. However, rear-wheel drive vehicles on low-friction surfaces exhibit significant degradation in stability when large drive torques are applied. Fig. 9 shows the vehicle behavior while applying drive and braking torques to the rear axle while cornering. This maneuver is intended to develop oversteer by reducing the available lateral force on the rear axle. A sequence of drive–brake–drive–brake torques at the actuator limits is used to provide multiple instances of excitation to test the controller. Fig. 9 shows the results from the maneuver and the controller parameters are again those given in Table II.

As with the previous figures, Fig. 9(a) is a plot of the yaw rate, sideslip angle, and lateral acceleration. Fig. 9(b) illustrates the yaw rate and rear slip angles along with their limits. In this case, the limits are a bit more interesting, as the rear wheel torque and speed profiles [seen in Fig. 9(d) and (e)] significantly affect the limits. For example, at approximately 22.5 s the accelerator is depressed to command maximum torque. The yaw rate and rear slip angle limits are instantly decreased since the MPC controller calculates that the maximum achievable values are lowered. However, the vehicle states cannot respond instantaneously, and so for several time

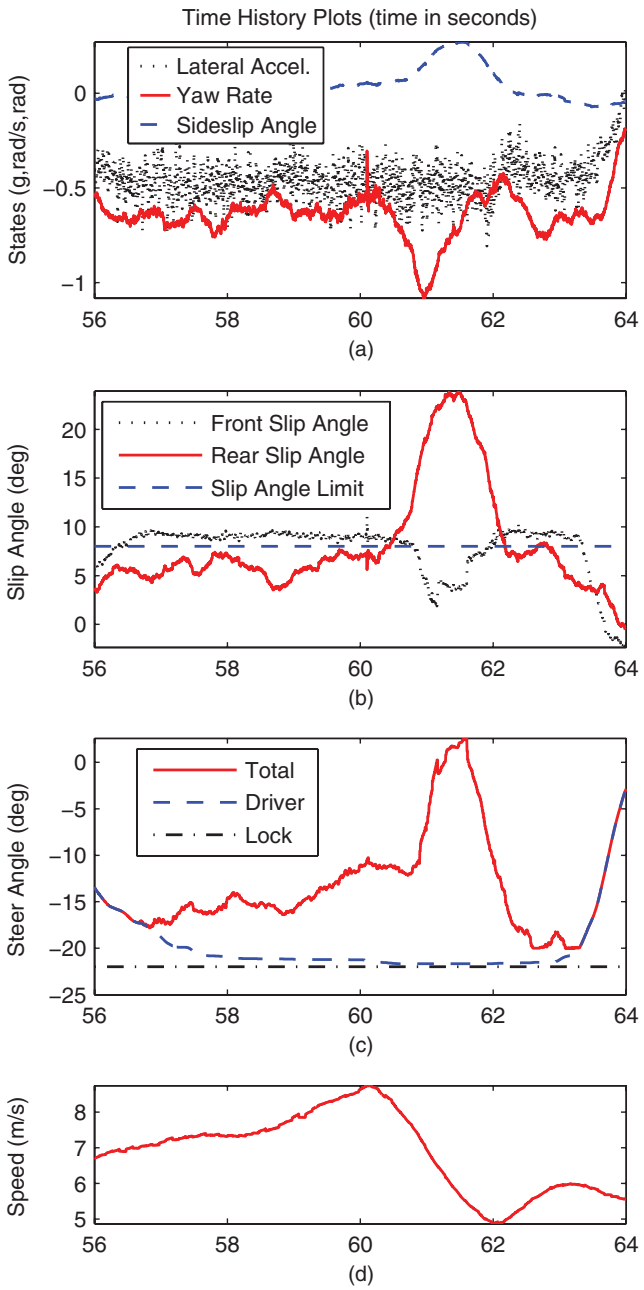

Fig. 10. Lift-off oversteer on low-μ surface. (a) States. (b) Slip angles. (c) Steering angles. (d) Speed.

steps the states are outside the new smaller envelope. The controller therefore countersteers hard to bring the states inside the envelope and then returns the vehicle again to the boundary, giving the driver the maximum possible cornering capability.

The representation of rear tire saturation and lateral–longitudinal force coupling in the AFI model (5) is critical in obtaining the performance of the envelope controller seen in Fig. 9. Without the prediction of decreased rear lateral force from the drive torque, the controller would be incapable of responding accurately to the rapid growth in rear slip angle. To illustrate the necessity of this information, a set of experiments were performed with a purely linear tire model used to predict the forces that would be developed on each axle. Fig. 10 demonstrates a lift-off oversteer on a mixed dirt and gravel surface. For this test, the model underlying the controller utilized a static linearization about zero slip angle at the rear axle and assumed a purely linear mapping between the front steering angle and the front lateral tire force. A front slip angle limit also replaced the yaw rate constraint. The parameters of this model, seen in Table III, were chosen to allow the tires to get to full saturation.

Fig. 10(a) shows the vehicle states throughout the maneuver. Note here that the vehicle has already entered a corner at 56 s when the timeline of the plot begins. The driver continues to increase the steering angle [seen in Fig. 10(c)] until reaching a limit understeering case where the controller countersteers to keep the front slip angle near the envelope boundary. There is a small steady-state error during the initial cornering phase as a result of the tire model overstating the effect of the steering input near tire saturation. Use of the AFI model avoids this by including the saturation dynamics in the steering angle calculation. When the driver applies drive torque to the rear axle, the rear slip angle increases dramatically. The controller countersteers, but the tire model mismatch results in a poor prediction of the dynamics in this highly nonlinear region and thus a violation of the envelope boundary occurs. Because the linear model has no representation of this tire saturation, the controller underestimates the steering input needed to stabilize the vehicle. The countersteer maneuver does eventually return the vehicle to the envelope, and the controller is successful in stabilizing the vehicle in the lift-off oversteer maneuver.

VI. Envelope Invariance Proof

A proof that the model predictive envelope controller stabilizes the vehicle, regardless of the driver input, is presented in this section. Since the controller is not easily expressed in a closed form, the proof is presented by examining the range of stabilizing inputs and showing that the optimization will produce these inputs as the MPC input to the vehicle.

The proof presented here leaves out the slew rate limits for clarity. The test vehicle used in experiments with the controllers described in this paper has an extremely fast steering system (see [16]) for which the slew rate constraints appear to be unrestrictive.

A general nonlinear two-state model is used throughout the proof to establish the feasibility of stabilizing the vehicle. The derivatives of this model match the derivatives of the AFI model at the boundaries of the envelope, allowing the discussion of the controller action at the limits of handling.

A. Theory of Exact Penalty Functions

It is common for a model predictive controller to contain, at its core, an optimization problem with both state and input constraints. As mentioned in the previous section, if both of these constraints are hard constraints, then the problem may be infeasible at some points. This can occur either due to the constraints being incompatible at some point in the state space or due to disturbances causing the states to deviate outside

the boundaries of the state constraints. In either case, the controller is incapable of determining a control action, so the constraints are softened in order to ensure problem feasibility. The drawback to softening the constraints is that the guarantee of controller action in the case that the original hard-bounded problem was feasible is lost. Fortunately, the theory of exact penalty functions provides a means to recover this guarantee.

In [18], the authors describe the use of exact penalty functions with a hard-constrained optimization problem of the form

$$\begin{aligned} \text{minimize} \quad & f(x) \\ \text{s.t.} \quad & g(x) \leq 0 \\ & h(x) = 0 \end{aligned} \tag{20}$$

where f, g, and h are functions from $\mathbb{R}^n$ into $\mathbb{R}$, $\mathbb{R}^m$, and $\mathbb{R}^k$, respectively. A point x in $\mathbb{R}^n$ satisfying the constraints is considered to be a feasible point. This problem can be reexpressed as an optimization problem with no constraints, but with a cost associated with any nonfeasible point

$$\text{minimize } f(x) + \alpha Q\left(||g(x)_+, h(x)||\right) \tag{21}$$

where α is a nonnegative real number, $g(x)_+$ is a penalty on any positive value of $g(x)$, and Q is a function that satisfies

$$Q(0) = 0 \quad Q(\zeta) > 0 \text{ for } \zeta > 0. \tag{22}$$

If $Q(\zeta) = \zeta$ and the 1-norm is used, then this problem becomes

$$\text{minimize } f(x) + \alpha \left(\sum_{j=1}^{m} g_j(x)_+ + \sum_{j=1}^{k} \left| h_j(x) \right| \right) \tag{23}$$

and is of exactly the same form used for the envelope control problem. The results presented in [18] demonstrate that, given this problem, there is a condition on the penalty weight that is defined by the dual norm of the Lagrange dual optimal inequality and equality multipliers λ and ν for the original problem. If $\alpha > \overline{\alpha}$ with

$$\overline{\alpha} = ||\lambda, \nu||_\infty \tag{24}$$

then a solution to the soft-bounded problem will also be a solution to the hard-bounded problem, provided that the hard-bounded problem is feasible.

The hard-constrained envelope control problem can be expressed as a standard-form quadratic program with linear constraints, which is

$$\begin{aligned} \text{minimize } & x^T P x + q^T x + r \\ \text{s.t.} \quad & A_1 x - b_1 \geq 0 \\ & A_2 x - b_2 = 0. \end{aligned} \tag{25}$$

Therefore, the Lagrange dual problem can be expressed as

$$\begin{aligned} \text{maximize } & r - \lambda^T b_1 - \nu^T b_2 \\ \text{s.t.} \quad & q + A_1 \lambda + A_2 \nu \\ & \lambda \geq 0. \end{aligned} \tag{26}$$

For each combination of A_1, A_2, b_1, b_2, q, and r, there is an associated condition on the penalty weight defined, as before, by the dual norm of the optimal multiplying factors, λ^* and ν^*. Since the desired soft-constrained problem uses the 1-norm to penalize the slack variables, the dual norm is the infinity-norm. Therefore, the condition needed for the envelope control problem slack weight is

$$\eta > \sup_{A_1, A_2, b_1, b_2, q, r} \left|\left| \lambda^*, \nu^* \right|\right|_\infty. \tag{27}$$

With respect to the envelope control problem, this establishes that, if the slack weight η is chosen to be sufficiently large and an input exists that prevents the vehicle from leaving the envelope, this input will be the solution to the optimization problem.

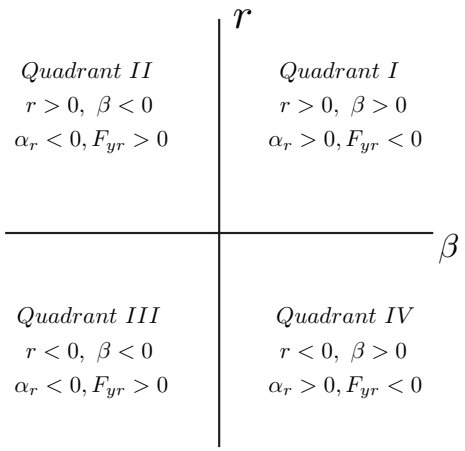

Fig. 11. Four quadrants of the state space used for the proof.

B. Feasibility of the Envelope

In order to determine whether a feasible input is present for all points on the boundary, the envelope is examined in each quadrant, as illustrated in Fig. 11. In quadrant I, the yaw rate and sideslip angle are both positive. Quadrant II contains states with positive yaw rates and negative sideslip angles. Quadrant III has negative yaw rates and sideslip angles and is symmetric to quadrant I. Finally, quadrant IV contains negative yaw rates and positive sideslip angles and is symmetric to quadrant II.

Beginning with quadrant II, in which open-loop equilibria for left turns lie, if they exist, the conditions for remaining in the envelope when on the boundary can be written as

$$\dot{r} \leq 0, \qquad \dot{\alpha_r} \geq 0. \tag{28}$$

If, at every point on the boundary, these conditions can be satisfied, then the model predictive controller can find an input that will, at the first time step, keep the states from exiting the boundary. At subsequent steps in the time horizon, the predicted states may move away from the linearization point. As such, there may be error in the prediction, but exits from the envelope will still be prevented since only the first time step will elapse before the solution is recomputed.

The conditions on the states must be expressed in terms of the input F_{yf} to ensure that they are feasible at every point on

the boundary of the envelope. Beginning with the yaw rate, a bound on the input F_{yf} is computed, as

$$\dot{r} = \frac{aF_{yf} - bF_{yr}}{I_{zz}} \leq 0 \quad \Longrightarrow \quad F_{yf} \leq \frac{b}{a}F_{yr}.$$

Given sufficient steering range on the vehicle, this condition is easily achievable since F_{yr} is positive in quadrant II and thus any negative F_{yf} is acceptable.

The rear slip angle derivative consists of a linear combination of the yaw rate and sideslip angle derivatives, and is thus more complicated than the yaw rate derivative. However, this can be handled in the same manner as the yaw rate derivative. Beginning with the expression for the rear slip angle derivative

$$\begin{aligned} \dot{\alpha_r} &= \dot{\beta} - \frac{b}{U_x}\dot{r} \geq 0 \\ \frac{F_{yf} + F_{yr}}{mU_x} - r - \frac{b}{U_x}\dot{r} &\geq 0. \end{aligned} \tag{29}$$

Since the yaw rate condition must simultaneously hold, $\dot{r}$ is known to be negative, and it is clear that with $\dot{r} \leq 0$, and m, U_x, I_{zz}, and F_{yr} all positive quantities, a somewhat conservative condition can be written as

$$\frac{F_{yf} + F_{yr}}{mU_x} \geq r. \tag{30}$$

On the boundary $\alpha_r = \alpha_{r_{\max}}$, the rear tire is already fully saturated, yielding $F_{yr} = F_{yr_{\max}}$. Considering the case where the input is chosen to yield the least restriction on the yaw rate, $F_{yf} = (b/a)F_{yr_{\max}}$, this reduces to

$$\frac{F_{yr_{\max}}\left(1 + \frac{b}{a}\right)}{mU_x} \geq r \tag{31}$$

which is the yaw rate boundary of the envelope. Therefore, when inside the bounds, a feasible input may always be found which will prevent the vehicle from leaving the envelope. The same result holds for quadrant IV by symmetry.

Quadrants I and III are considered pathological cases of the vehicle control scheme since these combinations of states can be possible only in transient cases and have not been observed in experiments by the authors. However, the dynamics of the controlled vehicle can be illustrated in the same way as with quadrants II and IV. In quadrant I, the slip angle condition changes sign, yielding the following conditions for maintaining the vehicle in the envelope:

$$\dot{r} \leq 0, \qquad \dot{\alpha_r} \leq 0. \tag{32}$$

Beginning with the yaw rate equation like in quadrant II, the same condition on the front lateral force may be derived

$$\dot{r} = \frac{aF_{yf} - bF_{yr}}{I_{zz}} \leq 0 \quad \Longrightarrow \quad F_{yf} \leq \frac{b}{a}F_{yr}. \tag{33}$$

However, unlike in quadrant II, the rear lateral force F_{yr} is negative. Therefore, at the positive slip angle boundary, the input F_{yf} must be saturated at its minimum value to meet the yaw rate condition. This yields $F_{yf} = (b/a)F_{yr}$ and $\dot{r} = 0$, Thus, while it is not possible to reduce the yaw rate everywhere, there is an input at every point on the boundary that prevents the yaw rate from growing and keeps the vehicle within the envelope.

This yaw rate condition also makes the analysis at the slip angle boundary simple. Since the best case input on the slip angle boundary yields $\dot{r} = 0$ with $F_{yf} = (b/a)F_{yr}$, these values may be substituted into the slip angle dynamics

$$\begin{aligned} \dot{\alpha_r} &= \dot{\beta} - \frac{b}{U_x}\dot{r} \leq 0 \\ \frac{F_{yf} + F_{yr}}{mU_x} - r - \frac{b}{U_x}\dot{r} &\leq 0 \\ \frac{F_{yr}\left(1 + \frac{b}{a}\right)}{mU_x} - r &\leq 0. \end{aligned} \tag{34}$$

In quadrant I, $F_{yr} \leq 0$ and $r \geq 0$, and thus the rear slip angle is reduced when the yaw rate condition is satisfied. Again, the same conditions hold in quadrant III by symmetry.

C. Statement of the Proof

Theorem 1: If the vehicle states are initially within the envelope, an input exists at every point on the envelope boundary that drives the system states to the interior of the envelope, and the penalty weight on the slack variables in the optimization problem is chosen according to (27), then the vehicle cannot leave the envelope.

Proof: Given that the vehicle starts inside the boundaries of the envelope, it is known from solving the appropriate linear programs that

$$10 \geq \eta > \sup_{A_1, A_2, b_1, b_2, q, r} \left|\left|\lambda^*, \nu^*\right|\right|_\infty. \tag{35}$$

The actual slack weight for the controller is set at 50 000 for good performance in cases with disturbances that result in the vehicle outside the boundaries. Thus, since the results demonstrate that an input exists on every point on the boundary that keeps the states from leaving the envelope, the hard-constrained problem is feasible. Therefore, the model predictive controller with sufficient slack weight will always select an input that preserves the invariance of the envelope.

If it is desired to accommodate error in the parameterization of the model, the invariance proof may be completed by shifting the boundaries of the envelope inward so that an inward-cutting trajectory of the real model may always be found on the envelope boundaries. However, this shift in the boundaries adds conservatism to the control action which is typically undesired for the operation of the real system. Outside the envelope, the controller has been observed to drive the states toward the interior of the envelope. Though a guarantee of this action is omitted for brevity, this behavior can also be utilized to account for short-term disturbances and variations in model parameters. ■

VII. Conclusion

The possibility of utilizing real-time friction and state feedback on production vehicles offers exciting opportunities for control of the dynamics at the limits of handling. With this information, it is possible to calculate boundaries of a safe handling envelope that prevents the vehicle from exhibiting undesirable behavior. While many such stable envelopes exist, the envelope presented in this paper eliminates regions of state

space that can be clearly defined as unstable, is motivated from straightforward phase-plane analysis, and utilizes dynamic boundaries that may be easily calculated in real time.

The model predictive envelope controller presented in this paper enforces the boundaries of the envelope smoothly and in coordination with the human driver. Key to obtaining good performance at the envelope boundaries is the AFI model developed for this controller. This model incorporates the nonlinearities of the front and rear axles in a convex formulation, allowing powerful convex optimization techniques to be applied to find the solution to the MPC problem. Because the model provides sufficient information about the tire behavior, the controller is capable of holding the vehicle on the edge of the boundary, allowing the driver to utilize the maximum handling capabilities of the vehicle.

When implemented on an experimental steer-by-wire research vehicle, results showed that the envelope controller was capable of operating in real time and responded appropriately in the case of disturbances and mismatch in the friction estimate. Qualitative feedback from a small group of test drivers indicated that the envelope could be made large enough to satisfy intrepid drivers while ensuring vehicle stability. Future development of this stabilization technique will focus on incorporating real-time estimation of vehicle sideslip angle and tire–road friction coefficient to allow the system to operate using sensors readily available on production vehicles.

ACKNOWLEDGMENT

The authors would like to thank project team members Y. Deguchi, S. Joe, and T. Matsuda, Nissan Motor Company, Ltd., Kanagawa, Japan. The authors also gratefully acknowledge J. Mattingley, Information Systems Laboratory, Stanford University, Stanford, CA, for providing his real-time embedded optimization algorithms.

REFERENCES

[1] J. N. Dang, "Statistical analysis of the effectiveness of electronic stability control systems," Dept. Transportation, NHTSA, Washington, DC, Tech. Rep. HS 810 794, Jul. 2007.

[2] A. T. Van Zanten, R. Erhardt, G. Pfaff, F. Kost, U. Hartmann, and T. Ehret, "Control aspects of the bosch-VDC," in *Proc. Int. Symp. Adv. Vehicle Control*, Jun. 1996, pp. 573–607.

[3] Y.-H. Hsu, S. Laws, and J. Gerdes, "Estimation of tire slip angle and friction limits using steering torque," *IEEE Trans. Control Syst. Technol.*, vol. 18, no. 4, pp. 896–907, Jul. 2010.

[4] M. M. Waldrop, "Flying the electric skies," *Science*, vol. 244, no. 4912, pp. pp. 1532–1534, 1989.

[5] Y.-H. J. Hsu and J. C. Gerdes, "Envelope control: Keeping the vehicle within its handling limits using front steering," in *Proc. 21st Int. Symp. Dynamics Veh. Roads Tracks*, Aug. 2009.

[6] P. Falcone, F. Borrelli, J. Asgari, H. E. Tseng, and D. Hrovat, "Predictive active steering control for autonomous vehicle systems," *IEEE Trans. Control Syst. Technol.*, vol. 15, no. 3, pp. 566–580, May 2007.

[7] P. Falcone, F. Borrelli, H. E. Tseng, J. Asgari, and D. Hrovat, "Linear time-varying model predictive control and its application to active steering systems: Stability analysis and experimental validation," *Int. J. Robust Nonlinear Control*, vol. 6, pp. 862–975, Jul. 2007.

[8] G. Palmieri, O. Barbarisi, S. Scala, and L. Glielmo, "A preliminary study to integrate LTV-MPC lateral vehicle dynamics control with a slip control," in *Proc. 48th IEEE Conf. Decision Control*, Dec. 2009, pp. 4625–4630.

[9] D. Bernardini, S. D. Cairano, A. Bemporad, and H. Tseng, "Drive-by-wire vehicle stabilization and yaw regulation: A hybrid model predictive control design," in *Proc. 48th IEEE Conf. Decision Control*, Shanghai, China, Dec. 2009, pp. 7621–7626.

[10] E. Fiala, "Lateral forces on rolling pneumatic tires," *Zeitschrift V.D.I.*, vol. 96, no. 29, pp. 973–979, Oct. 1954.

[11] S. Boyd and L. Vandenberghe, *Convex Optimization*. Cambridge, U.K.: Cambridge Univ. Press, 2004.

[12] J. Mattingley and S. Boyd, "Automatic code generation for real-time convex optimization," in *Convex Optimization in Signal Processing and Communications*, Y. Eldar and D. P. Palomar, Eds. Cambridge, U.K.: Cambridge Univ. Press, 2009.

[13] J. Mattingley and S. Boyd, "Real-time convex optimization in signal processing," *IEEE Signal Process. Mag.*, vol. 27, no. 3, pp. 50–61, May 2010.

[14] M. Diehl, H. J. Ferreau, and N. Haverbeke, *Nonlinear Model Predictive Control*. Berlin, Germany: Springer-Verlag, 2009.

[15] J. Ryu and J. C. Gerdes, "Integrating inertial sensors with GPS for vehicle dynamics control," *J. Dynamic Syst., Meas., Control*, vol. 126, pp. 243–254, Jun. 2004.

[16] S. M. Laws, C. D. Gadda, and J. C. Gerdes, "Frequency characteristics of vehicle handling: Modeling and experimental validation of yaw, sideslip, and roll modes to 8 Hz," in *Proc. Int. Symp. Adv. Veh. Control*, Taipei, Taiwan, Aug. 2006, pp. 901–906.

[17] Y.-H. J. Hsu and J. C. Gerdes, "The predictive nature of pneumatic trail: Tire slip angle and peak force estimation using steering torque," in *Proc. Int. Symp. Adv. Veh. Control*, Kobe, Japan, Oct. 2008, pp. 1–6.

[18] S. P. Han and O. L. Mangasarian, "Exact penalty functions in nonlinear programming," *Math. Program.*, vol. 17, no. 1, pp. 251–269, 1979.

Craig Earl Beal received the B.S. degree in mechanical engineering from Bucknell University, Lewisburg, PA, and the Master's and Ph.D. degrees in mechanical engineering from Stanford University, Stanford, CA.

He is currently an Assistant Professor and the Jane W. Griffith Fellow with Bucknell University (through AY2015). While at Stanford University, he focused on vehicle dynamics and control as well as modular vehicle design and construction. While at Bucknell University as an Undergraduate Researcher, his research involved animatronics and pulse-width control for precision positioning of robots. His current research interests include the application of control systems to vehicle dynamics to improve safety, stability, and performance of vehicles in conjunction with human drivers.

Dr. Beal was a recipient of the Stanford Graduate Fellowship and the Tau Beta Pi National Scholarship.

J. Christian Gerdes is an Associate Professor with the Department of Mechanical Engineering and, by courtesy, with the Department of Aeronautics and Astronautics, Stanford University, Stanford, CA. He is the Director of the Center for Automotive Research, Stanford University. Currently, his students are involved in projects ranging from autonomous racing of by-wire vehicles to the modeling and control of homogeneous charge-compression ignition engines. Prior to joining Stanford, he was the Project Leader for virtual proving grounds development with the Vehicle Systems Technology Center, Daimler-Benz Research and Technology, Portland, OR. His current research interests include feedback control techniques for mechanical systems with a focus on improving vehicle safety and efficiency.

He was a recipient of the Presidential Early Career Award for Scientists and Engineers, the Rudolf Kalman Award from the American Society of Mechanical Engineers, and the Ralph R. Teetor Award from the Society of Automobile Engineers International.